Dependence of radar quantitative precipitation estimation error on the rain intensity in the Cévennes region, France

Guy Delrieu[a], Laurent Bonnifait[a], Pierre-Emmanuel Kirstetter[a] & Brice Boudevillain[a]

[a] Laboratoire d'étude des Transferts en Hydrologie et Environnement, BP 53, F-38041, Grenoble Cedex 9, France
Published online: 06 Jan 2014.

PLEASE SCROLL DOWN FOR ARTICLE

Dependence of radar quantitative precipitation estimation error on the rain intensity in the Cévennes region, France

Guy Delrieu, Laurent Bonnifait, Pierre-Emmanuel Kirstetter and Brice Boudevillain

Laboratoire d'étude des Transferts en Hydrologie et Environnement, BP 53, F-38041 Grenoble Cedex 9, France
guy.delrieu@ujf-grenoble.fr

Abstract Radar quantitative precipitation estimates (QPEs) were assessed using reference values established by means of a geostatistical approach. The reference values were estimated from raingauge data using the block kriging technique, and the reference meshes were selected on the basis of the kriging estimation variance. Agreement between radar QPEs and reference rain amounts was shown to increase slightly with the space–time scales. The statistical distributions of the errors were modelled conditionally with respect to several factors using the GAMLSS approach. The conditional bias of the errors presents a complex structure that depends on the space–time scales and the considered geographical sub-domains, while the standard deviation of the errors has a more homogeneous behaviour. The estimation standard deviation of the reference rainfall and the standard deviation of the errors between radar and reference rainfall were found to have the same magnitude, indicating the limitations of the available network in terms of providing accurate reference values for the spatial scales considered (5–100 km^2).

Key words Mediterranean heavy precipitation; weather radar; quantitative precipitation estimation; error model; space and time scales; GAMLSS

Dépendance de l'erreur d'estimation des lames d'eau radar à l'intensité de pluie dans les Cévennes, France
Résumé Les estimations quantitatives de pluie par radar (EQP radar) sont évaluées par rapport à une référence selon une approche géostatistique. Les valeurs de référence sont déduites de mesures pluviométriques en utilisant le krigeage de bloc. Les mailles de référence sont choisies en fonction de la variance d'estimation du krigeage. La cohérence entre EQP radar et pluie de référence augmente légèrement avec les échelles spatio-temporelles. Les distributions conditionnelles des erreurs sont modélisées en fonction de l'intensité de pluie par l'approche GAMLSS. Le biais conditionnel des erreurs a une structure complexe en fonction des échelles spatiales et temporelles ainsi que des domaines spatiaux considérés, alors que l'écart-type de l'erreur a un comportement spatialement plus homogène. L'écart-type d'estimation de la référence et l'écart-type de l'erreur sont du même ordre de grandeur, ce qui montre les limitations du réseau pluviographique disponible pour les échelles spatiales considérées (5–100 km^2).

Mots clefs précipitations méditerranéennes intenses; estimation quantitative des pluies; modèle d'erreur; échelles spatiales et temporelles; GAMLSS

INTRODUCTION

Characterization of the error structure of radar quantitative precipitation estimates (QPEs) is a major issue for applications such as assimilation of radar data in numerical weather prediction (NWP) models (Caumont *et al*. 2006, Berenguer and Zawadzki 2008)

and forcing of hydrological models with distributed rainfall data (e.g. Creutin *et al*. 1997, Ciach and Krajewski 1999, Ciach *et al*. 2007, Habib *et al*. 2008, Germann *et al*. 2009, Villarini *et al*. 2009, Kirstetter *et al*. 2010). One possible approach, referred to as a "physical approach" hereafter, is to examine all sources of errors (Villarini and Krajewski 2010)

separately and evaluate their cumulative effects. Pellarin *et al.* (2002) proposed the "hydrologic visibility" concept to quantify QPE systematic bias for radar systems operating in mountainous regions as a function of radar parameters (e.g. beam width, radar location and operating protocol). Berenguer and Zawadzki (2008) studied the full error covariance matrix of radar rainfall estimates by considering a large set of high-resolution S-band radar data and concomitant drop-size distribution (DSD) measurements. They focused on the combined errors associated with the transformation of reflectivity into rain rate and increasing beam broadening as a function of range in stratiform rainfall. Such a physical approach was particularly relevant to the objective of these authors, which was to assimilate raw radar data into NWP models. However, they recognized that the approach would become hardly tractable if additional error sources had to be considered, e.g. for shorter radar wavelengths due to the effects of attenuation. In addition, sophisticated data processing algorithms (Germann *et al.* 2006, Tabary 2007, Tabary *et al.* 2007, Delrieu *et al.* 2009) are now generally implemented in operational practice to cope with such error sources and increase the quality of radar QPEs. The physical approach is therefore also limited by the impact of the processing algorithms on the radar data sets. In other words, the radar QPE error structure is also *radar data processing dependent*.

The other approach consists of comparing radar QPEs with external reference values to characterize the overall error structure. Such a "product-error-driven" approach has been implemented many times in the past using reference values derived from data of dense raingauge networks (e.g. Delrieu *et al.* 1988), most recently for the NEXRAD system (Ciach *et al.* 2007, Krajewski *et al.* 2009, Seo and Krajewski 2011) in the USA and the Cévennes-Vivarais Mediterranean Hydro-meteorological Observatory in France (Kirstetter *et al.* 2010). Figure 1, which will be discussed in detail further on in this article, displays two examples of scatter plots between radar QPEs and reference rain amounts for two pairs of space–time scales (5 km^2, 1 h; 50 km^2, 12 h). Note that (a) the agreement between the two variables increases with the space and time scales; (b) the characteristics of the mean and variance of the error vary as a function of the reference rainfall value; and (c) conditional bias may exist at certain scales, e.g. for the 1-h time step (slight mean overestimation of the radar QPE between 20 and 40 mm, significant underestimation above 40 mm), and not at others, e.g. for the 12-h step.

Based on the above considerations, this study aims to establish conditional probability distribution functions of radar errors over a range of spatial (5–100 km^2) and temporal (1–12 h) scales. The reference rainfall is estimated in a geostatistical framework, making it possible to assess its accuracy. We want to study the dependence of the radar errors on several factors, primarily the rain intensity (or rain amount) and radar range, using a new approach based on Generalized Additive Models for Location, Scale and Shape (GAMLSS) proposed by Rigby and Stasinopoulos (2005). In the next section we present the context of our study and the associated data set. In subsequent sections, we discuss the reference rainfall and the radar error model, followed by a summary and conclusions.
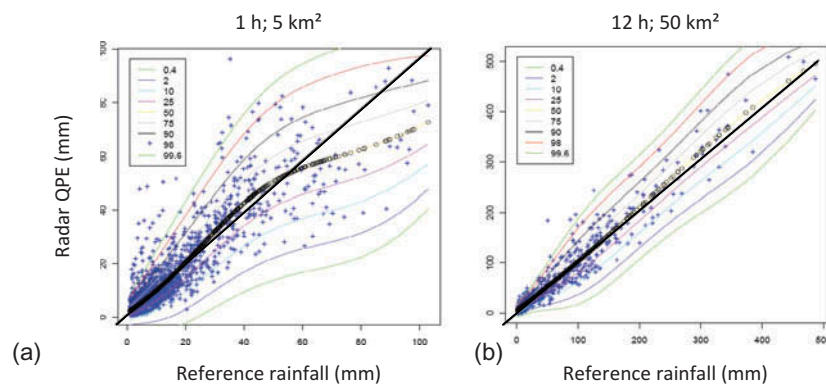
Fig. 1 Scatter plots of radar QPEs *vs* reference rainfalls for the space–time scales (a) 1 h; 5 km^2 and (b) 12 h; 50 km^2. The conditional distributions are established with the GAMLSS approach, assuming a Gaussian distribution of the errors. The conditional mean is represented by the black-dot curve and the 1:1 line by the thin solid line.

CONTEXT AND DATA SET

A detailed description of the Cévennes-Vivarais Mediterranean Hydrometeorological Observatory (CVMHO) is given by Boudevillain *et al*. (2011). Figure 2 shows the region of interest and the rainfall observation systems used herein, which include: (a) the S-band weather radar system of the Météo France ARAMIS network at Bollène; and (b) an hourly raingauge network with 252 raingauges over the 32 000 km^2 of the CVMHO window. Three events that produced major road traffic disturbances in part of the region (the Gard department) in 2007 and 2008 were selected for the present study (Fig. 3). Due to its extraordinary magnitude, the catastrophic event of 8–9 September 2002 (Delrieu *et al*. 2005, Bonnifait *et al*. 2009) was included in the following analyses. Radar QPEs were obtained with the TRADHy software (Traitements Régionalisés
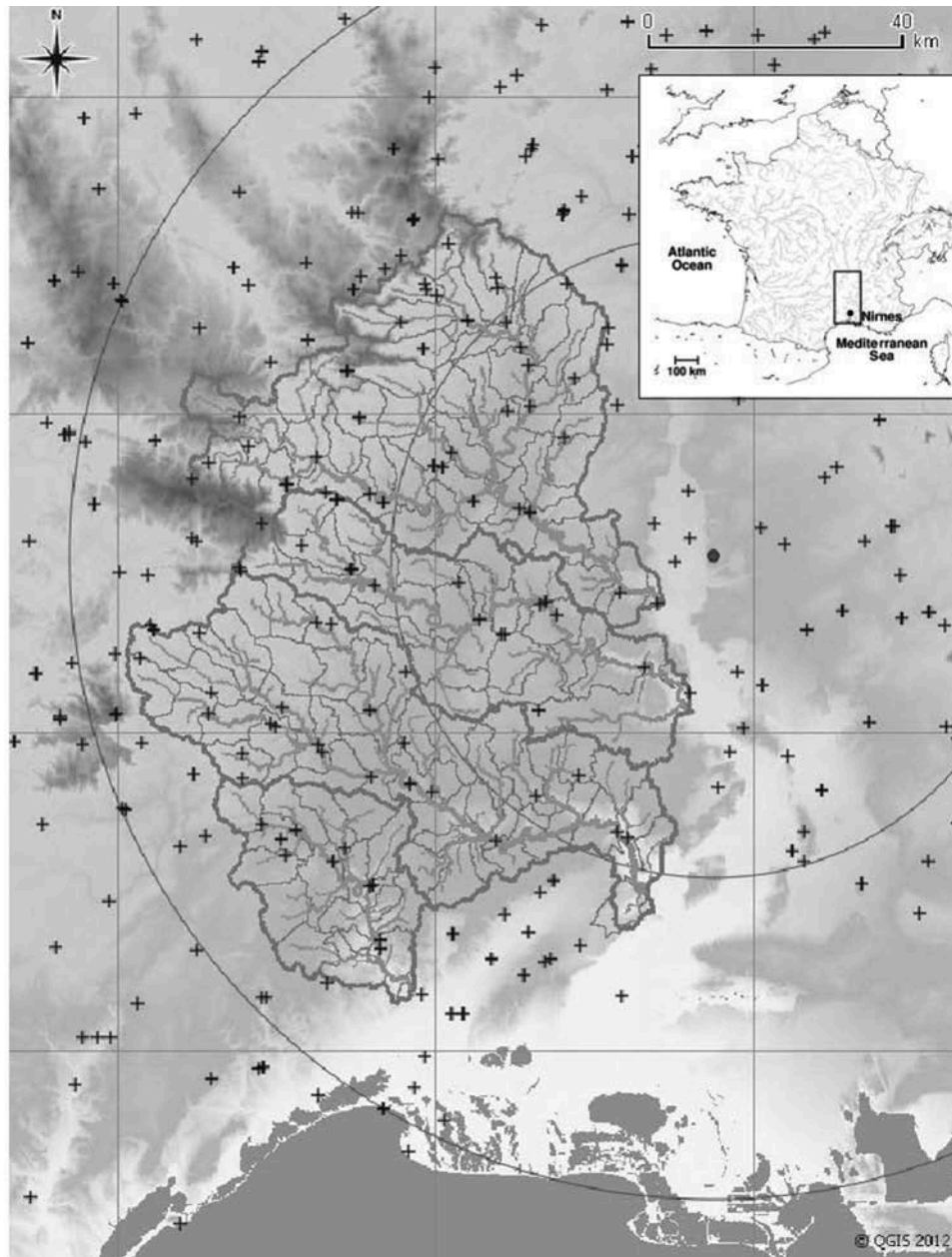
Fig. 2 Location of the CVMHO window in France (insert) together with a map of the rainfall observation system superimposed on the topography and the main catchments of the Cévennes region. The + signs refer to the hourly raingauge network; the radar pictogram and the 50-km range markers refer to the Météo France Bollène radar. The four main catchments (Ardèche, Cèze, Gardon, Vidourle from top to bottom) are subdivided into hydrological meshes of about 50 km^2.

$$R_{AT} = \int\limits_T \int\limits_A R(\underline{x}, t)\, \mathrm{d}\underline{x}\, \mathrm{d}t \tag{1}$$

where R denotes the true rainfall intensity at a given location $\underline{x}$ and time t.

The radar QPEs to be assessed are determined for a grid with a good spatial resolution of typically 1 km^2. Therefore radar QPEs over area A may be expressed as:

$$R_{AT}^* = \frac{1}{N_A} \sum_{i=1}^{N_A} R_T^*(a_i, t) \tag{2}$$

where a_i is the area of a radar pixel, N_A the number of pixels in area A and R_T^* the radar estimated rain amount falling over a time interval T centred at time t.

To establish the reference rainfall amounts, denoted R_{AT}^{ref}, from the raingauge network data, we used the block kriging technique (Journel and Huijbregts [1978](#), Goovaerts [1997](#)) with:

$$R_{AT}^{\mathrm{ref}} = \sum_{i=1}^{N_g} \lambda_i G_T(\underline{x}_i,\ t) \tag{3}$$

where $G_T(x_i, t)$ is the raingauge amount at point $\underline{x}_i$ for time interval T centred at time t and N_g is the number of raingauges accounted for in the estimation. The coefficients $\{\lambda_i,\ i = 1,\ N_g\}$ are the kriging weights obtained by minimizing the estimation variance:

$$\sigma_{\mathrm{ref}}^2 = \mathrm{E}(R_{AT}^{\mathrm{ref}} - R_{AT})^2 \tag{4}$$

under unbiasedness condition:

$$\mathrm{E}(R_{AT}^{\mathrm{ref}}) = E(R_{AT}) \tag{5}$$

The definite advantage of this geostatistical method over other interpolation techniques is that the estimation variance (equation (4)) provides a measure of the accuracy of the reference values that depends on the spatial structure of the variable to be estimated and the relative configuration of the network and the area of interest (A).

The availability of such a metric leads naturally to consider the residuals (rather than the ratios for instance) between the estimated and reference values as the working variable of the radar error model, with:

$$\Delta_{AT}^{\mathrm{ref}} = R_{AT}^* - R_{AT}^{\mathrm{ref}} = \Delta_{i,k} \tag{6}$$

Fig. 3 Rainfall maps obtained at the event time scale from the raingauge network (anisotropic kriging) for the four rain events. The visualization windows (black boxes) have been sized to the spatial extent of each rain event. The rainfall isolines are spaced at 100 mm, except for the 29–30 September rain event (50 mm).

et Adaptatifs de données radar pour l'Hydrologie; regionalized and adaptive radar data processing for hydrological applications, Delrieu *et al.* 2009), which copes with orogenic and anthropic clutter, beam shielding, rain partitioning into convective and stratiform rainfall, and the subsequent vertical profile of reflectivity identifications and corrections. Regarding bias correction, an "effective" Z–R relationship was optimized for each single event so as to minimize the bias and the conditional bias between radar and raingauge estimates at the event time scale following the approach proposed by Bouilloud *et al.* ([2010](#)).

REFERENCE RAINFALL

Problem formulation and spatial estimation of reference rainfall amounts

The true unknown rainfall amount falling on a given area, A, centred at point $\underline{x}$, over a given time interval T, centred at time t, can be expressed as:

where i indexes a given integration domain of size A and k a time step of duration T.

The kriging technique utilizes the variogram function:

$$\gamma_T(h) = \frac{1}{2}\, \mathrm{E}(R_T(\underline{x},t) - R_T(\underline{x+h},t))^2 \qquad (7)$$

to model the spatial correlation of the rain fields; here h denotes a horizontal distance and R_T the point value of the rain amount over a duration T. From rain-gauge data collected in the Cévennes region, Lebel *et al.* (1987) have established the following empirical model for the de-correlation distance (range of the variogram) as a function of the time interval considered:

$$d = 25\, T^{0.3} \qquad (8)$$

with d the distance in km and T the time in h, leading to de-correlation distances of about 25, 43 and 64 km for durations of 1, 6 and 24 h, respectively. This shows that the spatial representativeness of raingauge measurements increases with the rainfall duration. The CVMHO raingauge data were critically analysed following the method described by Kirstetter *et al.* (2010). Next, several kriging techniques (Goovaerts 1997) were implemented:

(a) ordinary kriging (OK) with the climatological variogram (equation (8)), assumed to be isotropic;
(b) OK with an isotropic variogram inferred for each time step from radar data; and
(c) OK with an anisotropic variogram inferred for each time step from radar data (Velasco-Forero *et al.* 2009).

No significant difference was found between the three methods in terms of performance assessed in a cross-validation exercise (not shown here for the sake of conciseness). Therefore, we use hereafter the simple climatological OK method to estimate the reference rainfall.

Selection of reference values based on the kriging estimation variances

The error model is built on the following principles: for a given landscape discretization into hydrological meshes of size A, we select a number of reference meshes for which the estimation is assumed to be good as the result of a good local raingauge coverage. For this purpose, we use the OK estimation

variance expressed, when optimized, by the following equation:

$$\sigma^2_{\mathrm{ref}} = -\gamma_{00} + \sum_i \lambda_i\, \gamma_{0i}\, + \mu \qquad (9)$$

where i indexes the intervening raingauges and μ is a Lagrange multiplier. Practically speaking, the integration domain is discretized into N_A Cartesian meshes, and the terms γ_{0i} and γ_{00} are estimated by:

$$\gamma_{0i} = \frac{1}{N_A} \sum_{j=1}^{N_A} \gamma_{ij} \qquad (10a)$$

and

$$\gamma_{00} = \frac{1}{N_A^2} \sum_{j=1}^{N_A} \sum_{k=1}^{N_A} \gamma_{jk} \qquad (10b)$$

Figure 4 gives two examples of the spatial discretization of four of the main Cévennes catchments (Ardèche, Cèze, Gardon, Vidourle) into hydrological meshes of 5 and 50 km^2. Also displayed in these maps are the normalized block kriging estimation variances (dimensionless quantities) for the 1-h time step using the climatological model (8): that is a variogram with a range of 25 km. The term "normalized" refers to the fact we have used a variogram sill equal to 1 in the calculations, while the variogram sill is theoretically equal to the field variance $\sigma^2_f(t)$. The maps of the normalized estimation variances summarize the estimation quality over the considered area. Clearly, the hydrological meshes containing (or located in the vicinity of) raingauges have low normalized estimation variances, while in the regions of low raingauge density (e.g. in the southeast part of the map), the normalized estimation variances reach values of about 0.6, whatever the spatial scale (5 or 50 km^2). For higher integration time steps, due to the increasing de-correlation distance (see equation (8)), the normalized estimation variances significantly decrease (not shown for the sake of conciseness).

We have arbitrarily chosen to select as reference values in the following, the OK values obtained over hydrological meshes with normalized estimation variances $\sigma^2_{\mathrm{refN}} < 0.1$. The following procedure is then used to de-normalize the estimation variances in order to express them in units of mm^2. Since the variogram sill is theoretically equal to the field variance, the reference estimation variances for a given time step and a given hydrological mesh can be expressed as:
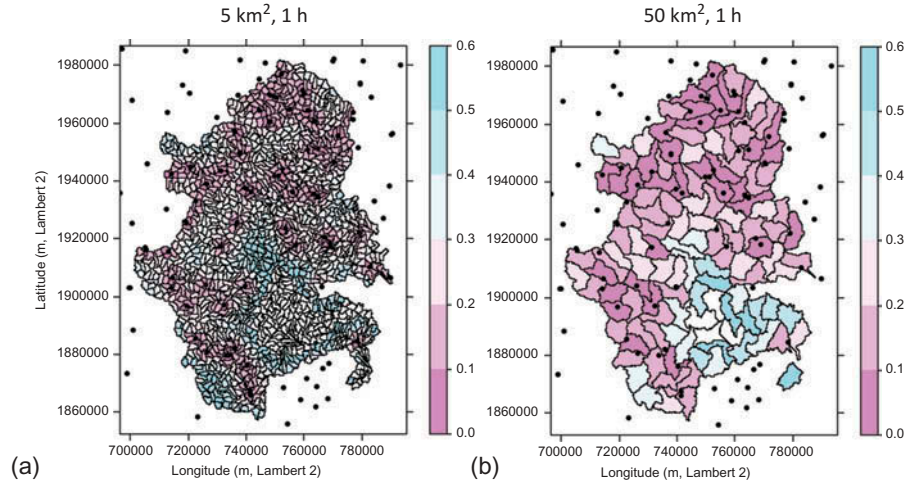
Fig. 4 Two examples of the spatial discretization of four of the main Cévennes catchments (Ardèche, Cèze, Gardon, Vidourle) into hydrological meshes of (a) 5 km^2 and (b) 50 km^2. Also displayed are the normalized ordinary kriging estimation variances for the 1-h time step using a climatological variogram model with a range of 25 km.

$$\sigma_{\mathrm{ref}}^2(A,T,t) = \sigma_f^2(T,t)\, \sigma_{\mathrm{refN}}^2(A,T,t) \qquad (11)$$

where $\sigma_f^2(T,t)$ is the field variance. For practical estimation, we consider the method proposed by Lebel *et al.* (1987) and already implemented by Kirstetter *et al.* (2010) for 1-km^2 integration areas in the CVMHO. According to this method, a linear regression is first established between the field standard deviation $\sigma_f(T,t)$ and the field mean $m_f(t)$ with:

$$\sigma_f(T,t) = a_T\, m_f(T,t) \qquad (12)$$

Then a local mean, denoted by $m_{AT}(t)$, is estimated for each hydrological mesh and time step, and used in the de-normalization procedure instead of the field mean to account for the non-stationarity of the rain field, through the following expression:

$$\sigma_{\mathrm{ref}}^2(A,T,t) = a_T^2\, m_{AT}(t)^2\, \sigma_{\mathrm{refN}}^2(A,T,t) \qquad (13)$$

Figure 5 displays the regression analyses between the field standard deviation and the field mean (equation (14)) for the 1-h and 12-h integration time steps. These graphs confirm the validity of the proposed linear relationship between these two variables. Figure 6 shows the resulting relationships between the de-normalized estimation standard deviations (equation (15)) and the reference rain amounts, for the reference hydrological meshes corresponding to the space–time scales of (5 km^2; 1 h) and (50 km^2; 12 h). The upper parts of the scatter plots are somewhat truncated due to the threshold considered on the normalized estimation variances ($\sigma_{\mathrm{refN}}^2 \leq 0.1$). Linear regressions are
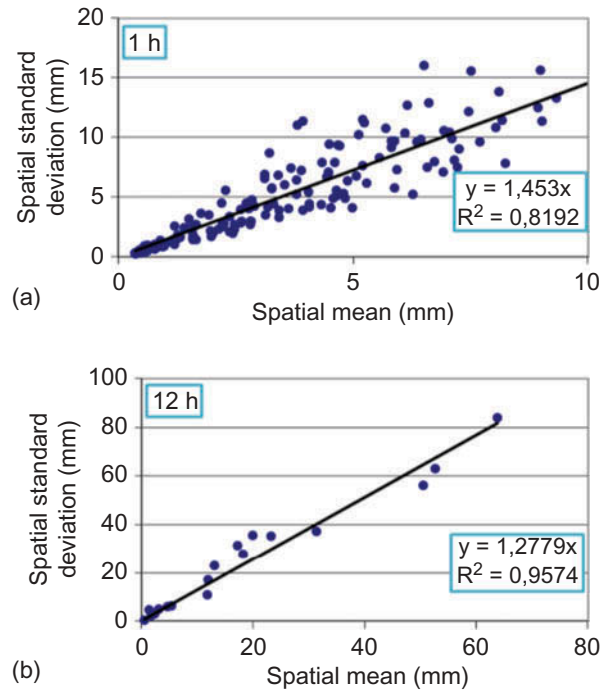
Fig. 5 Spatial standard deviation of the rain fields as a function of the spatial mean for two integration time steps: (a) 1 h and (b) 12 h.

found to satisfactorily represent the overall trends. As expected, there is a significant decrease in the slopes of such relationships when the space–time scales increase (0.347 and 0.254 for the two cases, respectively). Such linear models will be used in the next section to compare the estimation standard deviations of the reference values with the standard deviations of the errors between radar QPEs and reference values.
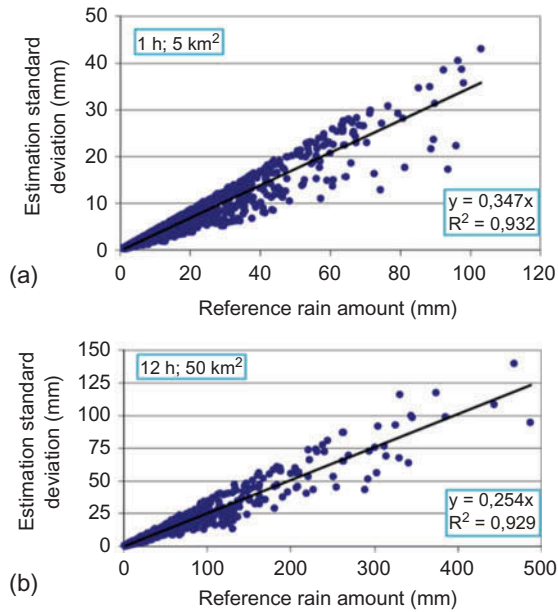
Fig. 6 Estimation standard deviation as a function of the rainfall value for the reference hydrological meshes for (a) the (1 h; 5 km^2) and (b) the (12 h; 50 km^2) space–time scales.

THE RADAR ERROR MODEL

Analysis of standard assessment criteria

Table 1 provides the values of standard assessment criteria between the radar QPE and OK reference values over a range of space–time scales (1, 2, 6 and 12 h; 5, 10, 50 and 100 km^2). The criteria used are the mean values of the two series, the coefficient of determination (square of the correlation coefficient) and the Nash-Sutcliffe efficiency. The means exhibit a consistent trend as a function of the space and time scales; their comparison shows a positive overall bias of the radar QPE, increasing from about 3.5% for the 1-h time step up to 9% for the 12-h time step. The coefficient of determination and Nash-Sutcliffe efficiency both show a slight but significant increase with increasing time step and/or hydrological mesh size.

To further discuss these results, Fig. 1, already referred to in the introduction, provides examples of the radar QPE *vs* reference rainfall assessment for two space–time scales. Visually, the results can be considered to be good for the (50 km^2, 12 h) case. Note that this is in part related to the optimization of an effective Z–R relationship for each single event performed so as to minimize the bias and conditional bias at the event time step. A complementary explanation comes from the good visibility of the Bollène radar for such well-developed convective events, especially those which took place in the plains of the CVMHO window (8–9 September 2002 and 29–30 September 2007). Unfortunately, the significant conditional bias observed for the (5 km^2, 1 h) case shows that the optimization of the Z–R relationship at the event time scale does not guarantee unbiased estimation in the conditional sense at shorter time scales. This problem of the scale dependence of the Z–R relationship, already identified by Krajewski and Smith (2004), may lead us to reconsider the Z–R optimization procedure used, which is

Table 1 Assessment criteria calculated between the radar QPEs and the climatological ordinary kriging reference rainfall for the four rain events overall. The selected reference hydrological meshes are those with a normalized estimation standard deviation $\sigma_{refN}^2 \leq 0.1$ whatever the space–time scale. (0,0) pairs are excluded from the criteria computations.

| Integration time step (h)	Integration domain size (km^2)	Radar QPE mean (mm)	Reference rainfall mean (mm)	Coefficient of determination	Nash-Sutcliffe efficiency	Sample size
1	5	12.1	11.7	0.79	0.78	3440
	10	11.5	11.1	0.80	0.80	2630
	50	10.5	10.1	0.82	0.80	1800
	100	10.1	9.6	0.84	0.82	1350
2	5	19.1	18.2	0.83	0.82	3930
	10	17.8	17.0	0.84	0.83	3080
	50	15.9	15.2	0.85	0.83	1860
	100	15.8	14.8	0.87	0.85	1180
6	5	42.5	40.2	0.88	0.87	3380
	10	39.5	37.2	0.88	0.87	2440
	50	35.9	33.2	0.90	0.88	1140
	100	35.5	32.6	0.91	0.89	650
12	5	63.3	58.3	0.91	0.90	2850
	10	61.1	56.1	0.92	0.90	1980
	50	58.6	54.2	0.93	0.91	770
	100	58.0	53.3	0.94	0.92	430

part of the (off-line) radar data processing system, e.g. by performing the optimization over a range of temporal scales. This example illustrates how a more detailed error model can be used to identify the weaknesses of the radar products and provide guidance to improve the processing algorithms. Here, we propose and illustrate a methodology to obtain such detailed assessments.

Conditional distributions of the errors (radar QPE – reference values)

We will extend the preliminary work of Kirstetter *et al.* (2010) on the characterization of the conditional distributions of the residuals $\Delta_{i,k}$, expressed by equation (6) between the radar QPE and the reference values, as a function of the reference values. Hereafter, the conditional distributions of the errors, denoted by $f_{AT}(\Delta \mid R^{\text{ref}})$, are established within the framework of the generalized additive models for location, scale and shape proposed by Rigby and Stasinopoulos (2005) and available in an R package called GAMLSS (Stasinopoulos *et al.* 2008). Such semi-parametric models consist of two components: a parametric probability density function (pdf) giving each value of the explanatory variable and a non-parametric relationship between the pdf parameters over the definition domain of the explanatory variable. The conditional densities are assumed to have the same parametric form for all values of the explanatory variable. The GAMLSS package offers a wide range of two-parameter (Gaussian, reverse Gumbel, gamma, log-normal, etc.) and three-parameter (exponential Gaussian, power exponential, t-family, etc.) continuous pdfs, as well as a number of non-parametric fitting techniques (cubic splines, penalised splines, loess function, etc.) for the second component of the model. The goodness-of-fit of a given model is assessed by investigating the so-called generalized Akaike information criterion (GAIC), a penalised function of the log-likelihood function to be minimized in the fitting procedure.

Figure 7 illustrates the fitting of the GAMLSS models for the errors as a function of the reference rainfall for three pdf models in the case of the (5 km^2, 1 h) space–time scales. Figure 7(a) corresponds to the fits obtained with the Gaussian pdf (NO hereafter):

$$f_1(y \mid \mu, \sigma) = \frac{1}{\sigma \sqrt{2\pi}} \exp\left(-\frac{(y - \mu)^2}{2\sigma^2}\right) \qquad (14)$$
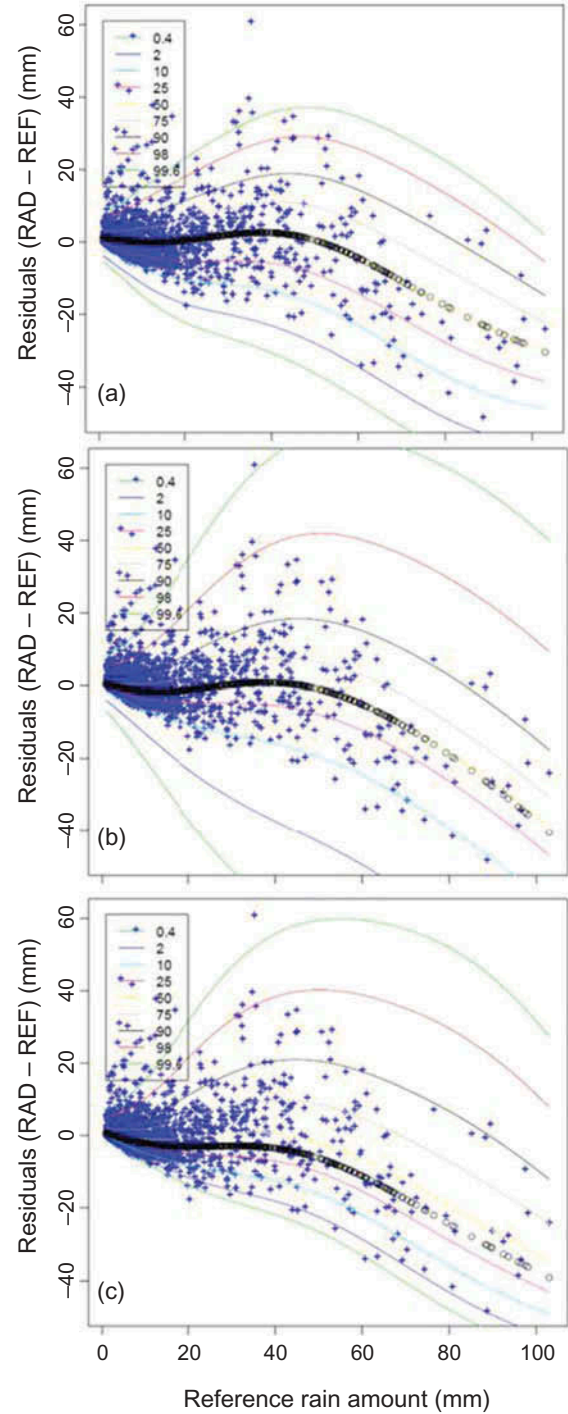
Fig. 7 Modelling the errors between radar QPEs and reference rainfall with the GAMLSS concept for the (1 h; 5 km^2) space–time scale under the assumption of (a) a Gaussian pdf, (b) a Power Exponential pdf and (c) a Reverse Gumbel pdf.

Figure 7(b) corresponds to those obtained with a symmetric three-parameter pdf called the power exponential pdf (PE), defined as:

$$f_2(y\,|\,\mu,\sigma,\nu) = \frac{1}{2c\sigma\,\Gamma(1/\nu)}$$
$$\times \exp\left(-\left|\frac{(y-\mu)}{c\sigma}\right|^{\nu}\right) \tag{15a}$$

with:

$$c^2 = \Gamma(1/\nu)/\,\Gamma(3/\nu) \tag{15b}$$

The PE distribution is suitable for leptokurtic as well as platykurtic data. Note that $\nu = 1$ and $\nu = 2$ correspond to the Laplace (i.e. two sided exponential) and normal distributions, respectively, while the uniform distribution is the limiting distribution as $\nu \to +\infty$.

Finally, the reverse Gumbel (RG) function (Fig. 7(c)) is a two-parameter pdf suitable for moderately positive skewed data:

$$f_3(y\,|\,\mu,\sigma) = \frac{1}{\sigma}\,\exp\left\{-\left(\frac{(y-\mu)}{\sigma}\right)\right.$$
$$\left. - \exp\left(-\frac{(y-\mu)}{\sigma}\right)\right\} \tag{16}$$

As a general trend for the fitting tests over all the space–time scales, the PE pdf was found to give better results than the NO pdf, or the other two- or three-parameter symmetric pdfs. As can be seen in Fig. 7(a) and (b), the PE fit corresponds to a leptokurtic case, a result consistent with the findings of Kirstetter *et al*. (2010) who indicated the Laplace pdf to be preferable to the Gaussian pdf in their case study. Among all the pdfs tested, the RG distribution was found to be the best compared with the symmetric distributions. This is likely due, in part, to the fact that the distribution of the residuals is inherently asymmetric: for a given reference value, the residual varies from $-R^{\mathrm{ref}}$ to $+\infty$. Note, however, the presence of a number of outlying high radar QPE values in the scatter plots, especially in the 0–20 mm range for the example of Fig. 7. This problem may be associated with residual clutter given the very high level of clutter observed in the considered mountainous region for the S-band frequency, as pointed out by Delrieu *et al*. (2009). Note that the performance of the log-normal distribution is lower (not shown here) than both the PE and RG distributions, and similar to the NO distribution. As can be seen in Fig. 7, the quantiles and conditional means resulting from these fits can be significantly different, especially between the symmetric
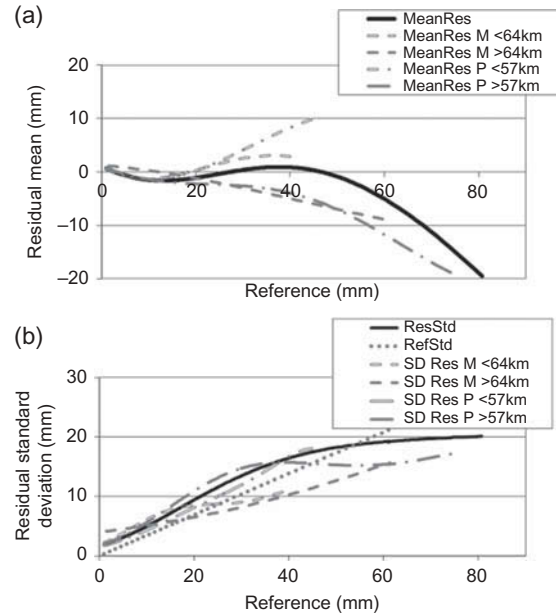
Fig. 8 (a) Mean and (b) standard deviation of the errors between the radar QPE and reference rainfall *vs* the reference rainfall for the (1 h; 5 km^2) space–time scales. The thick black curves correspond to the results for the entire set of reference meshes while the grey dashed curves correspond to the mountainous and plain parts of the region for two radar ranges. In addition the dotted line in the bottom figure presents the trend of the estimation standard deviation of the reference rainfall for the selected reference meshes.

and asymmetric pdfs. The above arguments led us to select the PE distribution for discussion of the results.

Figures 8 and 9 present the mean and standard deviation of the errors (i.e. the residuals) as a function of the reference rainfall for the (1 h, 5 km^2) and (12 h, 50 km^2) space–time scales, respectively. In addition to the results obtained by considering all the hydrological meshes overall for the four rain events, a segregation of the results is proposed for the mountainous (*M*) and plain (*P*) parts of the CVMHO window, and for two radar ranges. The values used to segregate according to radar range are different for the mountainous and plain regions, respectively 64 km and 57 km, to allow homogeneous sampling of the resulting four geographical domains ($M < 64$ km, $M > 64$ km, $P < 57$ km and $P > 57$ km) in terms of the number of reference meshes. To account for the sampling issue, we curtailed each plot at the reference value above which there are only about 10 data points. Concerning the error means (Figs. 8(a) and 9(a)), note that the results are quite different in terms of conditional bias for the two space–time scales, as already
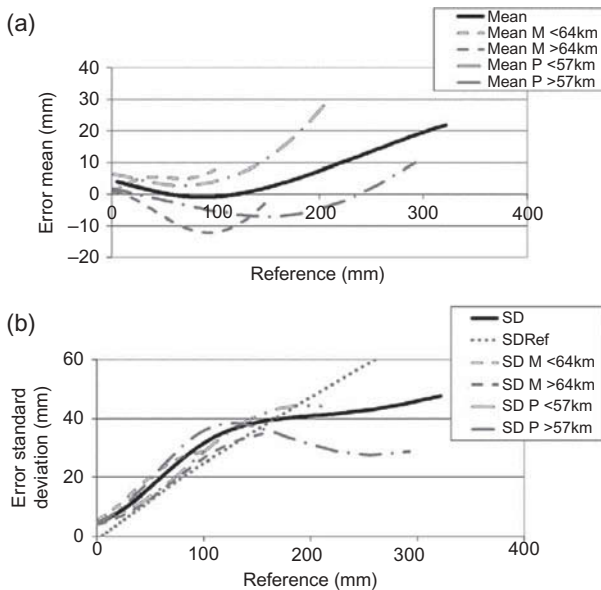
Fig. 9 (a) Mean and (b) standard deviation of the errors between the radar QPE and reference rainfall *vs* the reference rainfall for the (12 h; 50 km^2) space–time scales. See Fig. 8 for explanation.

noted in Fig. 1. From these graphs, two trends can be observed:

(a) There is a positive conditional bias for the $P < 57$ km region for the highest rain amounts at both time scales, while the bias remains moderate in the $M < 64$ km region.

(b) The behaviour of the error means is quite similar at the longer ranges for both the mountainous and plain regions—marked negative conditional bias for the (1 h, 5 km^2) scales; slight positive conditional bias for the (12 h, 50 km^2) scales. This similarity may be explained by the significant vertical extent of the considered rain systems that limits the effect of the mountain range on their visibility.

The above two points illustrate the fact that the range-dependent effects are not fully corrected for by the radar data processing system, with an underestimation at longer ranges for the 1-h time step, compensated for (by means of the Z–R relationship optimization) by an overestimation at closer range in the plain.

Concerning, the standard deviations of the errors, note that they increase more or less linearly between 0 and about one third of the maximum reference value, then sampling issues and the choice of the non-parametric method used to adjust the GAMLSS model (penalised splines) lead to a stabilization or a decrease. There is no distinct behaviour between the

results obtained for the different regions. The most striking feature is probably that the standard deviation of the errors between the radar and the reference values are similar to the estimation standard deviation of the reference values: in other words, the available raingauge network does not provide a very reliable reference for the space scales considered in this work. This is very different from the case of Kirstetter *et al*. (2010), who obtained reliable reference values (in that the estimation standard deviations of the reference values were significantly lower than those of the errors between radar and reference values) for 1-km^2 meshes containing raingauges. This is an indication of the strong decrease in the spatial representativeness of raingauges as the spatial scale increases, even for the longer time step (12 h) considered in this study.

SUMMARY AND CONCLUSION

In the present work, a geostatistical approach was implemented to establish reference values from raingauge data to assess radar QPEs in the context of Mediterranean heavy precipitation events. The main catchments of the region were divided into hydrological meshes of varying sizes (from 5 to 100 km^2). The reference values were estimated using the climatological OK technique by selecting reference meshes presenting normalized estimation variances of less than 0.1. Such meshes generally contain raingauge(s) or are located in the vicinity of raingauges. In a second step, the estimation variances were de-normalized using a technique based on the statistical link that exists between the standard deviation and the mean of the rain fields. With such a method, estimation variances can then be associated with each estimate to assess the quality of the estimation, or can be modelled as a function of the reference rainfall for overall assessment, which was the objective of our study.

After establishing the reference values and their estimation variances, the radar QPEs were compared to the reference values over a range of spatial and temporal scales (1–12 h; 5–100 km^2) using a number of classical criteria: bias, coefficient of determination and Nash-Sutcliffe efficiency. As expected, the agreement increases slightly as the space–time scales increase. The statistical distributions of the errors between estimated and reference values, conditional on the reference rainfall, were then modelled in detail by means of the so-called generalized additive models for location, scale and shape. It was found that the power exponential probability density function

(pdf), a three-parameter symmetric pdf, provides a better fit compared to the Gaussian pdf, with a more leptokurtic behaviour. The Reverse Gumbel pdf, a two-parameter moderately positive skewed pdf, was generally found to be superior to the symmetric pdfs, probably due to the inherent asymmetry of the residuals and the presence of radar QPE outliers associated with phenomena such as residual clutter. The conditional bias of the errors presents a complex structure as a function of the space and time scales, and as a function of the radar range and the considered geographical sub-domains (mountain *vs* plain). The standard deviation of the errors naturally decreases as the space and time scales increase; its evolution as a function of the reference rainfall is less influenced, compared to the bias, by radar range and geographical considerations. Importantly, the comparison of the estimation standard deviation of the reference rainfall and the standard deviation of the errors between radar and reference rainfall indicates that the available raingauge network is not dense enough to provide an accurate reference for the space scales considered, which are those useful for hydrological prediction in the region of interest.

Defining a radar error model therefore remains a complex topic, since such a model depends on the way radar data are processed, the space and time scales, the radar range and the topographic features of the region of interest. In addition, the sample size impacts on the robustness of the statistical analysis, especially for the highest rain rates. Due to their complementarity and inherent limitations, future work will be devoted to better conciliating the physical and product-error-driven approaches. We will also consider the implications of the dependencies of the error shown in this work on the generation techniques that can be used to obtain radar rainfall ensembles.

REFERENCES

Berenguer, M. and Zawadzki, I., 2008. A study of the error covariance matrix of radar rainfall estimates in stratiform rain. *Weather Forecasting*, 23 (6), 1085–1101.

Bonnifait, L., *et al*., 2009. Hydrologic and hydraulic distributed modelling with radar rainfall input: reconstruction of the 8–9 September 2002 catastrophic flood event in the Gard region, France. *Advances in Water Resources*, 32, 1077–1089.

Boudevillain, B., *et al*., 2011. The Cévennes-Vivarais Mediterranean Hydrometeorological Observatory database. *Water Resources Research*, 47, doi:10.1029/2010WR010353.

Bouilloud, L., *et al*., 2010. Radar rainfall estimation in the context of post-event analysis of flash floods. *Journal of Hydrology*, 394, 17–27.

Caumont, O., *et al*., 2006. A radar simulator for high-resolution nonhydrostatic models. *Journal of Atmospheric and Oceanic Technology*, 23, 1049–1067.

Ciach G.J. and Krajewski, W.F., 1999. On the estimation of rainfall error variance. *Advances in Water Resources*, 2, 585–595.

Ciach, G.J., Krajewski, W.F., and Villarini, G., 2007. Product-error-driven uncertainty model for probabilistic quantitative precipitation estimation with NEXRAD data. *Journal of Hydrometeorology*, 8, 1325–1347.

Creutin, J.D., Andrieu, H., and Faure, D., 1997. Use of weather radar for the hydrology of a mountainous area. Part II: radar measurement validation. *Journal of Hydrology*, 193 (1–4), 26–44.

Delrieu, G., Bellon, A., and Creutin, J.D. 1988. Comparative study of areal rainfall estimation methods using rain-gauge and radar data—application to daily rainfall events observed in the Montreal region. *Journal of Hydrology*, 98, 315–344.

Delrieu, G., *et al*., 2005. The catastrophic flash-flood event of 8–9 September 2002 in the Gard region, France: a first case study for the Cevennes-Vivarais Mediterranean Hydrometeorological Observatory. *Journal of Hydrometeorology*, 6, 34–52.

Delrieu, G., *et al*., 2009. Bollène 2002 experiment: radar rainfall estimation in the Cevennes-Vivarais region. *Journal of Applied Meteorology and Climatology*, 48, 1422–1447.

Germann, U., *et al*., 2006. Radar precipitation measurement in a mountainous region. *Quarterly Journal of the Royal Meteorological Society*, 132, 1669–1692.

Germann, U., *et al*., 2009. Real-ensemble radar precipitation estimation for hydrology in a mountainous region. *Quarterly Journal of the Royal Meteorological Society*, 135 (639), 445–456.

Goovaerts, P., 1997. *Geostatistics for natural resources evaluation*. Oxford: Oxford University Press.

Habib, E., Aduvala, A.V., and Meselhe, E.A., 2008. Analysis of radar-rainfall error characteristics and implications for streamflow simulation uncertainty. *Hydrological Sciences Journal*, 53 (3), 568–587.

Journel A. and Huijbregts, C., 1978. *Mining geostatistics*. London: Academic Press.

Kirstetter, P.E., *et al*., 2010. Toward an error model for radar quantitative precipitation estimation in the Cévennes-Vivarais region, France. *Journal of Hydrology*, 394, 28–41.

Krajewski, W.F. and Smith, J.A., 2002. Radar hydrology—rainfall estimation. *Advances in Water Resources*, 25, 1387–1394.

Krajewski, W.F., Villarini, G., and Smith, J.A., 2009. Radar rainfall uncertainties—where are we after thirty years of effort? *Bulletin of the American Meteorological Society*, 91, doi:10.1175/2009BAMS2747.1.

Lebel, T., *et al*., 1987. On the accuracy of areal rainfall estimation: a case study. *Water Resources Research*, 23 (11), 2123–2134.

Pellarin, T., *et al*., 2002. Hydrologic visibility of weather radar systems operating in mountainous regions: case study for the Ardeche Catchment (France). *Journal of Hydrometeorology*, 3, 539–555.

Rigby, R.A. and Stasinopoulos, D.M., 2005. Generalized additive models for location, scale and shape. *Journal of the Royal Statistical Society, Series C, Applied Statistics*, 54, 507–554.

Seo, B.-C. and Krajewski, W.F., 2011. Investigation of the scale-dependent variability of radar-rainfall and rain gauge error correlation. *Advances in Water Resources*, 34 (2), 152–163.

Stasinopoulos, D., Rigby, B., and Akantziliotou, C., 2008. *Instructions on how to use the GAMLSS package in R*. 2nd ed. Available at: http://studweb.north.londonmet.ac.uk/~stasinom/papers/gamlss-manual.pdf.

Tabary, P., 2007. The new French operational radar rainfall product. Part 1: Methodology. *Weather and Forecasting*, 22 (3), 393–408.

Tabary, P., Desplats, J., and Do Khac, K., 2007. The new French operational radar rainfall product. Part 2. *Weather and Forecasting*, 22 (3), 409–427.

Velasco-Forero, C.A., *et al.*, 2009. A non-parametric automatic blending methodology to estimate rainfall fields from rain gauge and radar data. *Advances in Water Resources*, 32 (7), 986–1002.

Villarini, G. and Krajewski, W.F., 2010. Review of the different sources of uncertainty in radar-based estimates of rainfall. *Surveys in Geophysics*, 31, 107–129.

Villarini, G., *et al.*, 2009. Product-error-driven generator of probable rainfall conditioned on WSR-88D precipitation estimates. *Water Resources Research*, 45, W01404, doi:10.1029/2008WR006946.